Noise-robust modal parameter identification and damage assessment for aero-structures

Gabriele Dessena
School of Aerospace, Transport and Manufacturing, Cranfield University, Cranfield, UK and
Department of Aerospace Engineering, Universidad Carlos III de Madrid, Leganés, Spain

Marco Civera
Department of Structural, Geotechnical and Building Engineering, Politecnico di Torino, Turin, Italy

Alessandro Pontillo
School of Engineering, University of the West of England, Bristol, UK, and

Dmitry I. Ignatyev, James F. Whidborne and Luca Zanotti Fragonara
School of Aerospace, Transport and Manufacturing, Cranfield University, Cranfield, UK

Abstract

Purpose – Ground vibration testing is critical for aircraft design and certification. Fast relaxed vector fitting (FRVF) and Loewner framework (LF), recently extended to modal parameter extraction in mechanical systems to address the computational challenges of time and frequency domain techniques, are applied for damage detection on aeronautically relevant structures.

Design/methodology/approach – FRVF and LF are applied to numerical datasets to assess noise robustness and performance for damage detection. Computational efficiency is also evaluated. In addition, they are applied to a novel damage detection benchmark of a high aspect ratio wing, comparing their performance with the state-of-the-art method N4SID.

Findings – FRVF and LF detect structural changes effectively; LF exhibits better noise robustness, while FRVF is more computationally efficient.

Practical implications – LF is recommended for noisy measurements.

Originality/value – To the best of the authors' knowledge, this is the first study in which the LF and FRVF are applied for the extraction of the modal parameters in aeronautically relevant structures. In addition, a novel damage detection benchmark of a high-aspect-ratio wing is introduced.

Keywords Modal analysis, Ground vibration testing, Modal parameters, Loewner framework, Fast relaxed vector fitting, Frequency domain, Noise, Damage detection, Structural health monitoring, Aeronautical structures, Aerospace structures, High aspect ratio wings

Paper type Research paper

Nomenclature

Definitions Acronyms and abbreviations

BeaRDS = Beam Reduction Dynamic Scaling;
EMA = Experimental modal analysis;
FRF = Frequency response function;
FRVF = Fast relaxed vector fitting;
GVT = Ground vibration testing;
HAR = High aspect ratio;
LF = Loewner framework;
LTI = Linear time-invariant;
MAC = Modal assurance criterion;
MOR = Model order reduction;
N4SID = Numerical algorithms for (4) subspace state space system identification;
OMA = Operational modal analysis;
SI = System identification;
SIMO = Single-input multi-output;
SHM = Structural health monitoring;
UAS = Unmanned aerial systems;
VF = Vector fitting;
XB-2 = eXperimental BeaRDS-2;
ζ_n = Damping ratios;
μ = Average or arithmetic mean;
ρ = Density;
φ_n = Mode shapes;
σ = Standard deviation; and
ω_n = Natural frequencies.

The current issue and full text archive of this journal is available on Emerald Insight at: **https://www.emerald.com/insight/1748-8842.htm**

Aircraft Engineering and Aerospace Technology
96/11 (2024) 27–36
Emerald Publishing Limited [ISSN 1748-8842]
[DOI 10.1108/AEAT-06-2024-0178]

Received 11 June 2024
Revised 26 July 2024
Accepted 27 August 2024

Introduction

System identification (SI) is a well-established field (Ljung *et al.*, 2020) with broad applications in various engineering domains. In structural dynamics, SI is primarily used to model systems by determining their modal parameters from experimental or operational data (Mugnaini *et al.*, 2022), a process known as modal analysis. Modal analysis includes two subdomains: Experimental modal analysis (EMA) (Dessena *et al.*, 2022a) and operational modal analysis (OMA) (Sibille *et al.*, 2023). OMA, particularly prevalent in civil engineering (Zanotti Fragonara *et al.*, 2017), involves extracting modal parameters from output-only data and is also used in aeronautics for taxi vibration testing (Al-Bess and Khouli, 2024). Nevertheless, this work focuses solely on EMA approaches with the scope of identifying modal parameters, such as natural frequencies (ω_n), damping ratios (ζ_n) and mode shapes ($\boldsymbol{\varphi}_n$). These parameters find applications in vibration-based damage detection (Civera *et al.*, 2022) and model updating (Dessena *et al.*, 2024a, 2024c). This work focuses on the former.

In terms of vibration-based damage detection, damage, defined as a change affecting the operational capability of the system (Farrar *et al.*, 2001), is detected through structural health monitoring (SHM), using a statistical pattern recognition strategy involving operational assessment, data acquisition, feature selection and damage evaluation. Modal parameters obtained from EMA, like ω_n and $\boldsymbol{\varphi}_n$, are crucial for vibration-based SHM (Rytter, 1993), with ω_n primarily assessing damage severity (Fan and Qiao, 2011) and $\boldsymbol{\varphi}_n$ supporting damage localisation. On the other hand, ζ_n is unsuitable as a damage indicator due to its dependence on non-structural factors (Civera *et al.*, 2021a). For a general SHM overview, refer to Sohn *et al.* (2004); for vibration-based SHM using modal data, see Rytter (1993).

In aeronautics, EMA plays a critical role in ground vibration testing (GVT), an essential procedure in civil aircraft design and certification of large aircraft (Lubrina *et al.*, 2014), as well as in unmanned aerial systems (UAS) design (Olejnik *et al.*, 2022). GVT can be conducted on entire vehicles (Prananta *et al.*, 2016) or specific components like wings or helicopter blades (Weber *et al.*, 2021), facilitating the validation of finite element models used in design processes (Promio *et al.*, 2018).

Current methods for extracting modal parameters face computational challenges. Issues arise from the ill-conditioning of fitting processes in the frequency domain (Lefteriu and Antoulas, 2009) and difficulties in handling large datasets in the time domain (Dessena *et al.*, 2023a). To address these challenges, the single-input multi-output (SIMO) techniques Loewner framework (LF) (Dessena *et al.*, 2023a) and fast relaxed vector fitting (FRVF) (Civera *et al.*, 2021a) were recently extended to the extraction of modal parameters from frequency domain data in mechanical systems. Hence, the scope of this work is threefold:

- Compare the LF and FRVF for noise robustness and damage detection application.
- Pioneeringly apply the LF and FRVF to vibration-based damage detection in aeronautical structures.
- Introduce a novel experimental benchmark case study of a high aspect ratio (HAR) wing with simulated damage.

Firstly, the robustness to noise is assessed on an original numerical dataset for increasing noise levels. The same dataset also features different damage and loading scenarios for the preliminary assessment of the vibration-based damage detection capability of LF and FRVF on aeronautically inspired synthetic structures. Then, the original experimental dataset of a HAR wing with simulated damage is introduced. For the numerical model, the identified parameters are compared to the numerical results and for the newly introduced experimental dataset, numerical algorithms for (4) subspace state space SI (N4SID) (Van Overschee and De Moor, 1994) are used as a benchmark. The performance of the methods is assessed in terms of precision of the identification and computational performance (time-to-identification in s).

The experimental data for the GVT of the HAR wing are made available to interested readers in an openly available Zenodo repository entry (Dessena, 2024).

Methods

A thorough review of the SI discipline, or its use for modal analysis, is not within the scope of this work and the interested reader is referred to the book (Ljung, 1987) for SI, and to the classical work (Maia, 1988) for the SI role in modal analysis. Nevertheless, an introduction to the two recently introduced SI methods used within this work, LF and FRVF, is given.

Fast and relaxed vector fitting

The FRVF, introduced in Deschrijver *et al.* (2008), refines the vector fitting (VF) algorithm (Gustavsen and Semlyen, 1999) for modelling large multiport electrical circuits. FRVF enhances VF by introducing a relaxed constraint during pole identification (Grivet-Talocia and Gustavsen, 2016; Gustavsen, 2006) and using $\boldsymbol{QR}$ decomposition (such that a matrix $\bar{\boldsymbol{A}} = \boldsymbol{QR}$ of an orthonormal matrix $\boldsymbol{Q}$ and an upper triangular matrix $\boldsymbol{R}$) for efficient matrix computation. In the form considered here, the FRVF procedure was tested and applied for the first time for the SI of simple mechanical systems in Civera *et al.* (2021b) and to large civil structures and infrastructures in Civera *et al.* (2021a).

FRVF is an iterative method. Following a linear least-squares approach, it relocates initial poles to minimise the divergence between estimated transfer functions and experimentally recorded data. That is to say, the complex-valued data $\boldsymbol{f}(s) \in C^{p\times k}$ (for k frequency samples, defined over $s = j\omega$ and for p frequency response functions [FRFs]) are approximated (for a generic single input-multiple outputs configuration) by the rational function:

$$\mathbf{f}(s) \approx \sum_{m=1}^{k} \frac{\mathbf{c}_m}{s - a_m} + \mathbf{D} + s\hat{\mathbf{e}} \tag{1}$$

where k is the preset number of poles to be identified, $\boldsymbol{a}_m$ is the mth pole (at any given iteration), $\boldsymbol{c}_m$ is the corresponding vector of residues, $\boldsymbol{D} \in \mathrm{R}^{p\times 1}$ is the feedthrough matrix (again, reduced to a column vector for a single input scenario) and $\hat{\boldsymbol{e}} \in \mathrm{R}^{p\times 1}$ contains the terms proportional to s (generally all zeroed and included here for completeness only). The poles are all complex conjugates, thus they come in pairs as $\boldsymbol{a}_m = -\alpha + j\beta$, $(a_m + 1) = -\alpha - j\beta$, where the real part is strictly negative (i.e.

they all lie in the left half of the complex plane) to ensure the stability of the dynamic system. For the first set of poles, β is linearly spaced over the frequency range of interest and $\alpha = \beta/100$. These represent the departing points for the iterative, deterministic optimisation procedure.

The components of the rational model described in equation (1) can then be seen as the parameters of the state-space model, such as:

$$\mathbf{f}(s) \approx \mathbf{C}(s\mathbf{I} - \mathbf{A})^{-1}\mathbf{B} + \mathbf{D} + s\widehat{\mathbf{e}} \tag{2}$$

where, according to the common terminology of state-space modelling, $\boldsymbol{A} \in \mathrm{C}^{k\times k}$ is the system coefficient matrix, $\boldsymbol{B} \in \mathrm{R}^{k\times 1}$ is the input matrix (which, for this application, is reduced to a column vector of ones) and $\boldsymbol{C} \in \mathrm{C}^{\mathrm{p}\times \mathrm{k}}$ is the output matrix. The VF identifies the poles of $\boldsymbol{f}(s)$ by solving (in the least-square sense) the following linear problem:

$$\sigma(s)\mathbf{f}(s) = \mathbf{p}(s) \tag{3}$$

where:

$$\sigma(s) = \sum_{m=1}^{k} \frac{\widetilde{\mathbf{c}}(s)}{\mathbf{s} - \mathbf{q}_m} + 1 \tag{4a}$$

$$\mathbf{p}(s) = \sum_{m=1}^{k} \frac{\widetilde{\mathbf{c}}(s)}{\mathbf{s} - \mathbf{q}_m} + \mathbf{D} + s\mathbf{E} \tag{4b}$$

indicate the mth tentative pole. In the fast and relaxed variant of the VF variant, the definition of $\boldsymbol{\sigma}(s)$ is slightly changed; specifically, it is relaxed as:

$$\sigma(s) = \sum_{m=1}^{k} \frac{\widetilde{\mathbf{c}}_m}{s - q_m} + \widetilde{\mathbf{D}} \tag{5}$$

where $\bar{\boldsymbol{D}}$ is real but not necessarily unity (even if it is expected to approach 1 as the procedure converges throughout the subsequent iterations). Thus, the pole relocation procedure aims at achieving the terms $\boldsymbol{p}_m$ that most closely resemble their (unknown) counterparts ($\boldsymbol{a}_m$), such that the root-mean-square error of approximation for $\boldsymbol{f}(s)$, i.e. the error of the fitting, is minimised.

More details concerning the implementation and the several technical aspects of FRVF can be found in (Grivet-Talocia and Gustavsen, 2016).

Loewner framework

The LF was first introduced as a SIMO SI technique for the extraction of modal parameters for vibration-based SHM of mechanical systems in the frequency domain in Dessena *et al.* (2023a).

The LF was notably proposed in Gosea and Antoulas (2015) as a model order reduction (MOR) technique for large dynamical systems, but its origins can be traced back to the 1930s, when Charles Loewner introduced the namesake interpolation matrix (L) (Löwner, 1934).

Antoulas *et al.* (2017; 2007) have developed the LF for the MOR of dynamical systems by considering tangential interpolation, or rational interpolation along tangential directions (Kramer and Gugercin, 2016). Later, they applied it to the SI of electronic systems in Lefteriu and Antoulas (2009) to relax the severely ill-conditioning of current fitting processes (Lefteriu and Antoulas, 2010).

Given a linear time-invariant dynamical system $\sum$ with k internal variables in time-continuous descriptor-form representation, m inputs and p outputs:

$$\sum : \mathbf{E}\frac{d}{dt}\mathbf{x}(t) = \mathbf{A}\mathbf{x}(t) + \mathbf{B}\mathbf{u}(t); \mathbf{y}(t) = \mathbf{C}\mathbf{x}(t) + \mathbf{D}\mathbf{u}(t) \tag{6}$$

where $\mathbf{x}(t) \in \mathrm{R}^{k\times 1}$ is the internal variable, $\boldsymbol{u}(t) \in \mathrm{R}^{m\times 1}$ is the function input and $\boldsymbol{y}(t) \in \mathrm{R}^{\mathrm{p}\times 1}$ is the output. The constant matrices for k internal variables are:

$$\mathbf{E}, \mathbf{A} \in \mathbb{R}^{k\times k}, \mathbf{B} \in \mathbb{R}^{k\times m}\mathbf{C} \in \mathbb{R}^{p\times k}\mathbf{D} \in \mathbb{R}^{p\times m} \tag{7}$$

When, for a given finite value λ, the matrix $\boldsymbol{A}$- $\lambda\boldsymbol{E}$ is non-singular, such that $\lambda \in \mathrm{C}$, a Laplace transfer function, $\boldsymbol{H}(s)$, of $\boldsymbol{\Sigma}$ can be defined in the form of a p by m rational matrix function:

$$\mathbf{H}(s) = \mathbf{C}(s\mathbf{E} - \mathbf{A})^{-1}\mathbf{B} + \mathbf{D} \tag{8}$$

The LF, via tangential interpolation, actively fits the FRF data to $\boldsymbol{H}(s)$. The aim does not differ from more established techniques, such as the rational fraction polynomial method, but the definition of the tangential interpolation directions (random in practice) allows for a more streamlined computation. A theoretical exposition of the LF is found in Mayo and Antoulas (2007), while the recent contributions to the implementation of the LF are outlined in full detail in Dessena *et al.* (2023a), a comparison of its computational performance is found in Dessena *et al.* (2023b) and a MATLAB tutorial is given in Dessena (2023a, 2023b).

Numerical case study

For comparing the robustness to noise of the LF and FRVF, a numerical case study of a wing spar of a small (maximum take-off mass <7 kg) fixed-wing UAS is introduced. The spar is discretised as a four-element two-dimensional Euler–Bernoulli cantilever beam in MATLAB by using standard (4 × 4) mass and stiffness matrices [see equations (A1a) and (b) in the Appendix], where the degrees of freedom are rotations (θ^{xy}) and vertical displacements (x_n), as shown in Figure 1(a). The spar square box cross-section is shown in Figure 1(b).

The beam is made from 6061-T6 aluminium with an elastic modulus (E) estimated at 70 GPa and a density (ρ) of 2,700 kgm^{-3}. The beam section dimensions are defined in Figure 1(b), while its length (L) is 1.1 m.

For comparing the SHM capabilities of LF and FRVF, five different scenarios exist for the spar:

1 baseline condition;
2 5% stiffness reduction in the third element;
3 10% stiffness reduction in the third element;
4 30% stiffness reduction in the third element; and
5 Pylon and engine at the spar's midpoint, discretised as a 0.3 kg lumped mass.

Figure 1 4-element beam: beam section and profile

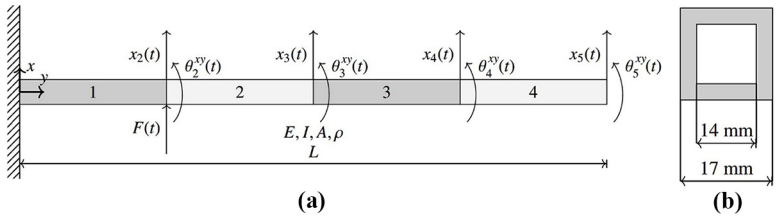

Notes: (a) The schematic drawing of the 4-element Euler–Bernoulli beam; (b) the schematic of the beam square box cross-section with the relative dimensions
Source: Created by authors

These were selected to have four progressive damaged scenarios and a change in mass configuration, which could mimic an under-wing payload or a pylon-engine assembly. The ζ_n is set to 3% for all cases and modes.

Investigation of noise effects

The LF and FRVF robustness to noise is tested by corrupting both input and output channels with additive white Gaussian noise at 0%, 0.1%, 0.2%, 0.5%, 1%, 1.5%, 2%, 3%, 4% and 5% of the signal standard deviation (σ), totalling ten independent cases per scenario. Because LF is a numerical method primed by random starting points, the tangential directions which are random in practice (Quero *et al.*, 2019), a numerical study over the ten noise cases for the five scenarios is carried out by running the identification 100 times (100 realisations) at the minimum order. This means that modes appearing in at least 90% of the realisations are considered. On the other hand, FRVF is a fully deterministic method; therefore, such a study is not needed. Nevertheless, FRVF is an iterative process; thus, for the scope of this work, the number of iterations was set to 5 at its minimum order. The minimum order of k for detecting eight modes for both LF and FRVF is 16 (e.g. number of systems poles).

Figures 2(a) and (b), compare the identified ω_n from LF and FRVF and the numerical values. The modes are considered identified if less than a 10% deviation from the expected numerical result is found. For brevity, only the results of scenarios # 1 and 5 are graphically presented as the behaviour in scenarios # 2–4 is similar to # 1.

In Figure 2(a), the LF demonstrates superior capability in identifying a wider range of modes than FRVF. However, LF struggles with higher modes as noise levels increase, unlike FRVF, which consistently identifies the first mode but is less reliable with modes 2–5. LF generally identifies correctly the ω_{1-5} across noise levels, with perfect identification in noiseless and 0.1% noise scenarios. Conversely, FRVF accurately identifies all modes in the first three noise cases except for the fifth scenario, where the first mode is correctly identified only in the noiseless case due to initial pole convergence challenges at lower frequencies when artificially added noise is present.

Concerning the ζ_n (shown as damping in %) of the stable modes, Figures 2(c)–(e) (LF) are more coherent with the expected values, when compared to Figures 2(d)–(f) (FRVF). LF consistently approaches the expected value across noise scenarios, while FRVF shows full consistency only in no and 0.1% noise cases, with partial coherence in the 0.2% case. The comparison of mode shapes $\boldsymbol{\varphi}_n$ via the modal assurance criterion (MAC) (Allemang and Brown, 1982) shows LF [Figures 2(g) and 2(i)] and FRVF [Figures 2(h) and 2(j)] results largely coherent with expected values, with LF showing more consistency overall.

In summary, the LF struggles with higher modes. However, the lower modes are identified inconsistently. Compared to the FRVF, the LF tends to produce more coherent results for damping ratios and mode shapes across noise levels.

Investigation of damage effects

This section compares LF and FRVF for damage detection using noiseless data, focusing on ω_n and $\boldsymbol{\varphi}_n$, while ζ_n remains constant. Figure 3(a) illustrates the percentage difference between $\omega_{1\text{-}3}$ identified by LF and FRVF for damaged cases relative to the baseline, confirming the sensitivity of both methods to damage detection, even for small damage scenarios. In addition, Figure 3(a) demonstrates close agreement between identified and numerical values. LF and FRVF effectively detect and localise small changes, with the largest deviations (in terms of modal displacement) occurring at the damaged elements. $\boldsymbol{\varphi}_1$ deviations increase with damage and mass addition, especially noticeable between nodes 3 and 4 [Figures 3(b)–(c)], demonstrating the suitability for both LF and FRVF SHM.

With regards to the time to identification, the performance of the two methods, for the minimum order $k = 16$, is reported. The mean (μ) and σ for the time to identification, are, respectively, 4.170 s (LF) and 0.375 s (FRVF) and 0.381 s (LF) and 0.264 s (FRVF). The statistical measures were computed over 50 identification realisations. The results are obtained from a Windows 11 desktop machine with an Intel® Xeon® Processor E5-1650 at 3.20 GHz and 32 GB of RAM. From the results, FRVF is both the least computationally demanding method and the most stable in time, because its σ is smaller than that from LF.

In conclusion, LF and FRVF succeed in identifying modal parameters under no or low noise conditions, with LF demonstrating greater resilience to higher noise levels. LF accurately predicts low and medium-frequency modes, while FRVF does better with high-frequency modes. LF robustness to noise enhances its efficiency in real-world applications, particularly for detecting structural changes like damage or added mass. Although FRVF outperforms LF in computational efficiency, the former identifies more stable

Figure 2 4-element beam: ω_n identified for scenarios # 1 and 5

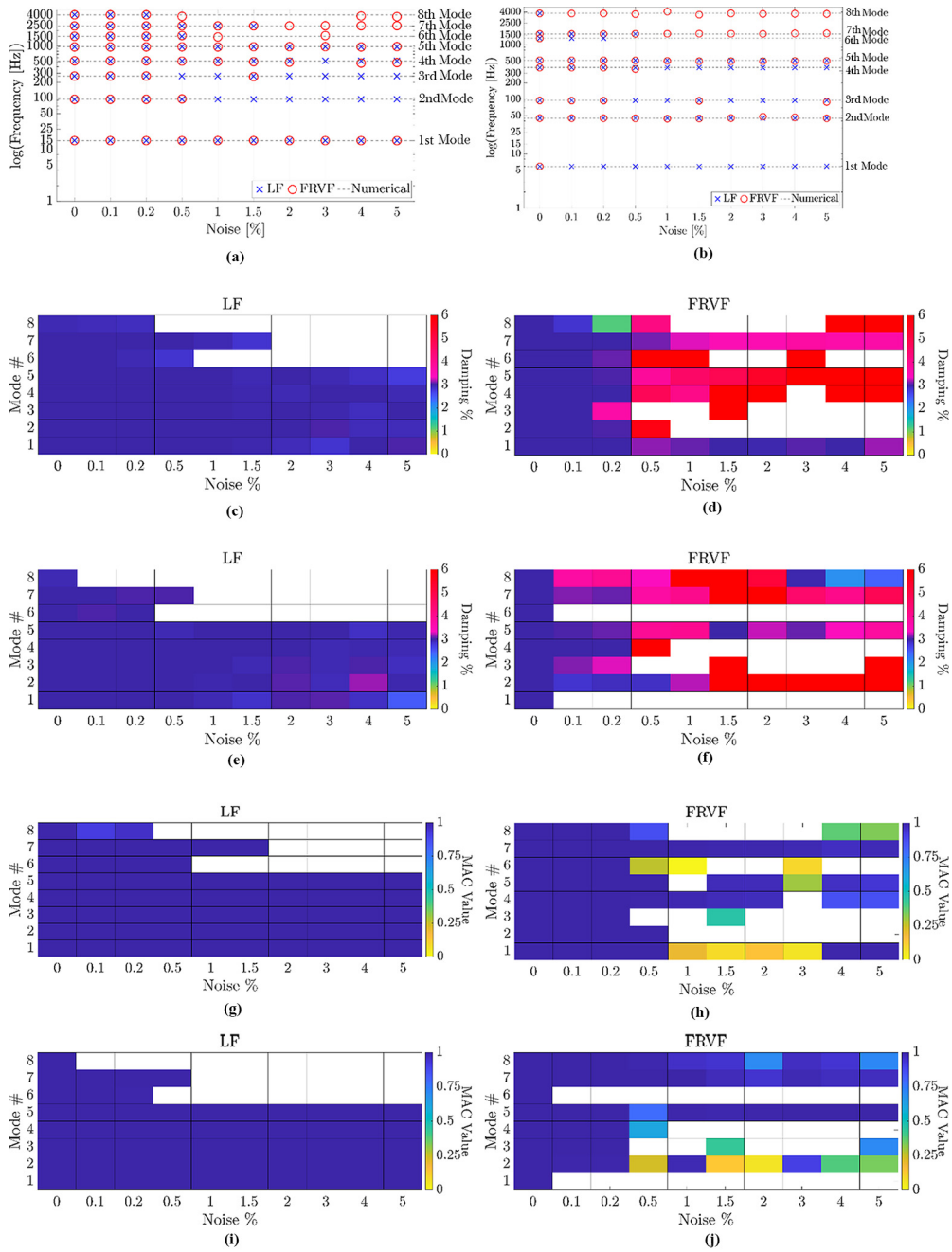

Notes: (a) and (b), ζn identified via LF (c) and (e) and FRVF (d) and (f) for, respectively, scenarios # 1 and 5 and the MAC of the identified φn via LF (g) and (i) and FRVF (h) and (j) for scenarios # 1 and 5

Source: Created by authors

modes across scenarios, indicating better identification capabilities.

Ground vibration testing of a flexible wing

After the successful implementation of LF and FRVF on a synthetic benchmark, a new experimental case study, based on the eXperimental BeaRDS-2 (XB-2) HAR wing (Figure 4) developed within the Beam Reduction Dynamic Scaling (BeaRDS) project at Cranfield University (Hayes *et al.*, 2019; Pontillo, 2020; Pontillo *et al.*, 2018; Yusuf *et al.*, 2019), is introduced.

The XB-2 wing was conceived as a dynamically scaled example of a civil jet airliner wing to be tested in the university

Figure 3 4-element beam: change in the identified $\omega_{1\text{-}3}$ *and* φ_1 wrt the damage scenario

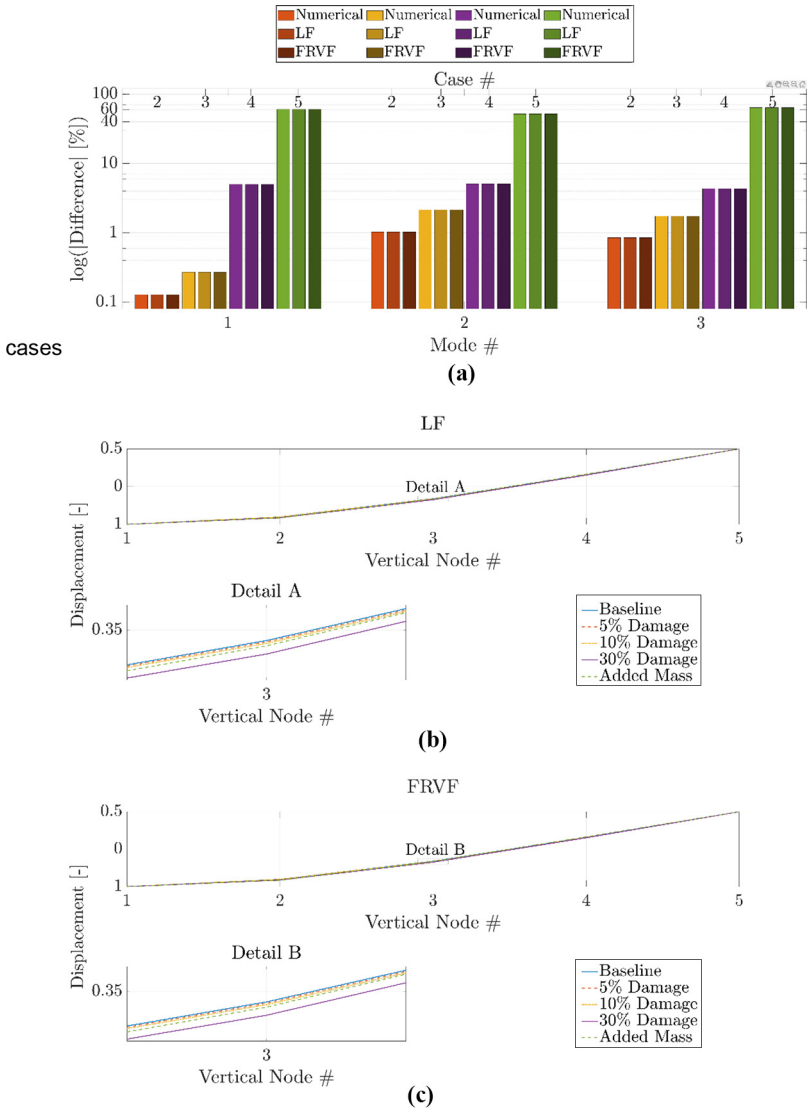

Notes: (a) Compares the ωn of the identified and numerical results from different scenarios; the modal displacement of φ1 of for the vertical component of all cases identified by LF (b) and FRVF (c) for the noiseless cases. The detailed views (details A and B) show a zoomed-in view of the mode shape
Source: Author's own creation

wind tunnel. The wing is made of three components: the spar, the stiffening tube and the skin.

The aerodynamic surface of the wing, outlined by a NACA 23015 aerofoil, has a span of 1.5 m (1.385 m from the origin in Figure 4), with a mean aerodynamic chord of 0.172 m, a taper ratio of 0.35, a leading-edge sweep of 1.49° and a mass of 3.024 kg. The wing has neutral twist and dihedral angles. The skin is responsible for transferring the aerodynamic loads to the underlying structure and is made of two 3D-printed plastics: Digital ABS and a rubber-like compound, Agilus 30. Combining a rigid and a rubber-like material allows the skin to be flexible and preserves structural integrity.

The wing torque box consists of the spar and tube assembly. The spar was machined from two 6082-T6 aluminium blocks which were welded together and secured with four bolted L-profile plates. The main spar features a Saint George cross-shaped cross-section and a variable taper along its span, while the tube is a stainless steel tube with a 10 mm diameter and 1 mm thickness.

For the scope of this work, four scenarios are considered. The specimen described above is considered the baseline and three loaded scenarios are introduced, as described below:

- Baseline: Total mass 3.024 kg;
- Added masses: 75 g at 1,010 mm, 12 g at 1,050 mm and 61 g at 1,365 mm – 3.172 kg;
- Added masses: 88 g at 1,010 mm, 51 g at 1,050 mm, 83 g at 1,205 mm and 61 g at 1,365 mm – 3.307 kg; and

Figure 4 XB-2 wing top view. *y*-axis coming out of the page

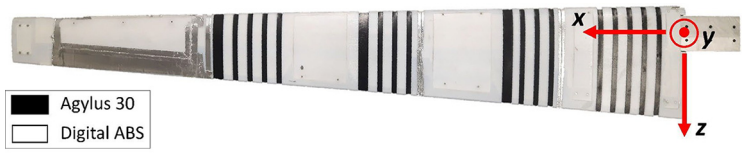

Source: Adapted from Dessena *et al*. (2024b) and Dessena(2023a)

- Added masses: same as Scenario 2 plus 181 g at 570 mm and 170 g at 665 mm – 3.658 kg.

The scenarios represent progressive addition of mass to simulate increasing damaged scenarios on the wing. The location and magnitude of the added mass are limited by the existing configuration of the wing, such as ballast mass fixing points and removable panels location.

The three loaded scenarios are introduced to assess LF and FRVF sensitivity to changes in aeronautical structures. In addition, the LF and FRVF results are compared with modal parameters extracted with the well-established method N4SID. From a previous modal survey (Dessena *et al.*, 2022b) involving the baseline wing, the first three dominant modes in the vertical direction were identified between 3 and 20 Hz. Hence, for this work, the frequency band for the linear sine sweep excitation was set between 2 and 25 Hz and spanned across 20 min (single sweep). The data is available in the data availability statement. A thorough description of the hardware setup is found in Dessena *et al.* (2022b).

Stabilisation diagrams help identify modal parameters from the experimental data, and Table 1 presents the results for the stable modes. LF and N4SID generally had the most stable diagrams, but even so, this did not undermine the precision of FRVF.

In Table 1, the stable ω_n and ζ_n identified with N4SID, LF and FRVF are presented. The identifications with LF and FRVF are mostly consistent with the N4SID benchmark results. In fact, the relative difference between the ω_n of LF and FRVF and those from N4SID never exceeds 1%, while the ζ_n is mostly under 10% and on rare occasions between 10% and 15%. However, this is expected due to the intrinsic nature of damping (Civera *et al.*, 2021b).

In general terms for $\boldsymbol{\varphi}_n$, the diagonal values of the MAC matrices – the off-diagonal terms have a negligible value – between the identified values from LF, FRVF and N4SID, for all cases, apart from $\boldsymbol{\varphi}_4$ in the baseline scenario for FRVF, exceed 0.95 (MAC = 0.89 for $\boldsymbol{\varphi}_4$ of the baseline scenario), which means an almost perfect correlation between the modes and presented methods. This is shown in Figure 5.

Figure 6 shows the $\boldsymbol{\varphi}_1$ identified by the three methods in the baseline and scenario # 4. A deviation from the baseline $\boldsymbol{\varphi}_1$ is displayed for all methods. In addition, a change is shown for all relevant positions (the three spanwise points corresponding to the accelerometer locations), accounting for the simulated damage localisation. Only the baseline and # 4 scenarios are shown for conciseness and clarity, but similar results are available for the other scenarios.

Conclusion

This study compares the LF and FRVF for modal parameter extraction from vibration data. Key findings include:

- FRVF is more affected by measurement noise but faster than LF by an order of magnitude.
- FRVF detects higher-order modes better, while LF identifies more modes accurately with precise damping estimation.
- LF provides more stable results with fewer spurious identifications.

Table 1 Natural frequencies and damping ratios identified by LF and FRVF for all scenarios

Mode	1st bending			1st coupled			2nd coupled		
Scenario	N4SID	LF	FRVF	N4SID	LF	FRVF	N4SID	LF	FRVF
Natural frequency [Hz]									
1	3.190	3.202	3.203	11.896	11.886	11.858	17.763	17.703	17.725
2	2.957	2.958	2.945	12.096	12.134	12.083	17.350	17.302	17.294
3	2.775	2.769	2.788	12.002	12.025	12.014	17.079	17.101	17.023
4	2.729	2.725	2.727	11.970	11.965	11.938	15.067	15.052	15.004
Damping ratio [−]									
1	0.032	0.040	0.028	0.066	0.063	0.065	0.058	0.061	0.062
2	0.021	0.024	0.025	0.060	0.057	0.058	0.061	0.056	0.060
3	0.019	0.022	0.021	0.058	0.055	0.057	0.050	0.050	0.057
4	0.019	0.021	0.019	0.050	0.048	0.052	0.046	0.039	0.038

Source: Created by authors

Figure 5 XB-2 wing: $\varphi_{1,2,4}$ identified by LF, FRVF and N4SID for the baseline scenario

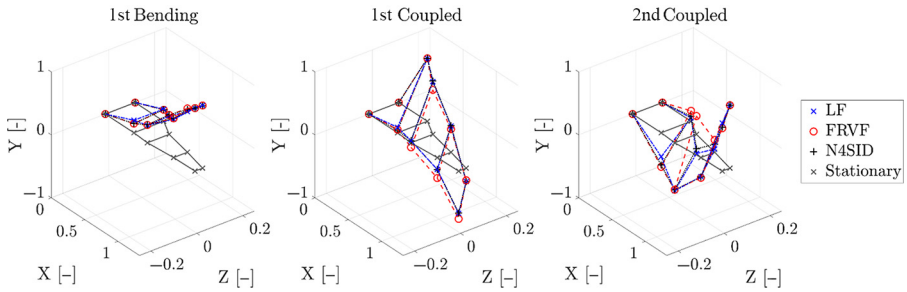

Source: Created by authors

Figure 6 XB-2 wing: φ_1 of the baseline and Scenario #4 identified by LF, FRVF and N4SID

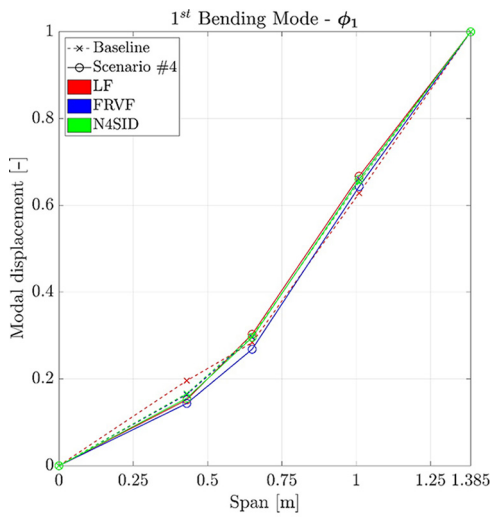

Source: Created by authors

- Both align with standard methods (N4SID), with FRVF slightly more accurate and LF more stable.
- Both detect damage and structural changes accurately.
- Furthermore, a novel benchmark for high-aspect-ratio wing damage assessment is introduced.

Acknowledgements

The authors wish to thank Dr Ivan Petrunin from the Centre for Autonomous and Cyber-Physical Systems at Cranfield University for providing the facilities and part of the equipment used for the tests and Prof Stefano Grivet-Talocia of the Department of Electronics and Telecommunications of the Politecnico di Torino for his valued advice.

Funding: The authors from Cranfield University disclosed receipt of the following financial support for the research, authorship and/or publication of this article: This work was supported by the Engineering and Physical Sciences Research Council (EPSRC) (grant number 2277626). The second author is financially supported by the Sustainable Mobility Center (*Centro Nazionale per la Mobilità Sostenibile* – MOST), Spoke 7 (Cooperative Connected and Automated Mobility and Smart Infrastructures), Work Package 4 (Resilience of Networks, SHM and Asset Management)

Author contributions: Conceptualisation, G.D. and M.C.; methodology, G.D., M.C. and A.P; software, G.D., M.C. and L.ZF.; validation, G.D., M.C., A.P., D.I.I. and J.F.W.; formal analysis, G.D. and M.C.; investigation, G.D.; resources, A.P., D.I.I., J.F.W. and L.ZF.; data curation, G.D. and M.C.; writing–original draft preparation, G.D.; writing–review and editing, G.D., M.C., A.P., D.I.I., J.F.W. and L.ZF.; visualisation, G.D., M.C. and D.I.I.; supervision, D.I.I., J.F. W. and L.ZF.; funding acquisition, L.ZF.

Conflict of interest: The author(s) declare none.

Data availability statement: Experimental data underlying this study can be accessed through the Zenodo Repository at https://doi.org/10.5281/zenodo.11635814 under the terms of under the terms of [GNU General Public License (GPLv3)].

References

Al-Bess, L. and Khouli, F. (2024), "Experimental investigation of a flexible airframe taxiing over an uneven runway for aircraft vibration testing", *SAE International Journal of Aerospace*, Vol. 17 No. 2, pp. 1-17, doi: 10.4271/01-17-02-0013.

Allemang, R.J. and Brown, D.L. (1982), "'A correlation coefficient for modal vector analysis", *Proceedings of the 1st International Modal Analysis Conference, Schenectady, New York, NY*, pp. 110-116.

Antoulas, A.C., Lefteriu, S. and Ionita, A.C. (2017), "'A tutorial introduction to the Loewner framework for model 'reduction", *Model Reduction and Approximation*, Society for Industrial and Applied Mathematics, Philadelphia, PA, pp. 335-376, doi: 10.1137/1.9781611974829.ch8.

Civera, M., Calamai, G. and Zanotti Fragonara, L. (2021a), "System identification via fast relaxed vector fitting for the structural health monitoring of masonry bridges", *Structures*, Vol. 30, pp. 277-293, doi: 10.1016/j.istruc.2020.12.073.

Civera, M., Calamai, G. and Zanotti Fragonara, L. (2021b), "Experimental modal analysis of structural systems by using the fast relaxed vector fitting method", *Structural Control and Health Monitoring*, Vol. 28 No. 4, pp. 1-23, doi: 10.1002/stc.2695.

Civera, M., Mugnaini, V. and Zanotti Fragonara, L. (2022), "Machine learning-based automatic operational modal

analysis: a structural health monitoring application to masonry arch bridges", *Structural Control and Health Monitoring*, Vol. 29 No. 10, pp. 1-23, doi: 10.1002/stc.3028.

Deschrijver, D., Mrozowski, M., Dhaene, T. and De Zutter, D. (2008), "Macromodeling of multiport systems using a fast implementation of the vector fitting method", *IEEE Microwave and Wireless Components Letters*, Vol. 18 No. 6, pp. 383-385, doi: 10.1109/LMWC.2008.922585.

Dessena, G. (2023a), "Identification of flexible structures dynamics", PhD thesis, Centre for Autonomous and Cyberphysical Systems, Cranfield University, Cranfield, UK, available at: https://dspace.lib.cranfield.ac.uk/handle/1826/20261]

Dessena, G. (2023b), "'A tutorial on the Loewner-based system identification and structural health monitoring approach for mechanical systems'", *School of Aerospace, Transport and Manufacturing*, Cranfield University, Cranfield, UK, doi: 10.17862/cranfield.rd.16636279, available at https://dspace.lib.cranfield.ac.uk/handle/1826/22465].

Dessena, G. (2024), *'Dataset: Structural Health Monitoring of a Flexible Wing'*, Cranfield University, Cranfield, UK, doi: 10.5281/zenodo.11635814, available at https://zenodo.org/records/12802077.

Dessena, G., Ignatyev, D.I., Whidborne, J.F. and Zanotti Fragonara, L. (2024a), "A global–local meta-modelling technique for model updating", *Computer Methods in Applied Mechanics and Engineering*, Vol. 418, p. 116511, doi: 10.1016/j.cma.2023.116511.

Dessena, G., Civera, M., Zanotti Fragonara, L., Ignatyev, D.I. and Whidborne, J.F. (2023a), "A Loewner-based system identification and structural health monitoring approach for mechanical systems", *Structural Control and Health Monitoring*, Vol. 2023, pp. 1-22, doi: 10.1155/2023/1891062.

Dessena, G., Ignatyev, D.I., Whidborne, J.F., Pontillo, A. and Zanotti Fragonara, L. (2022a), "Ground vibration testing of a flexible wing: a benchmark and case study", *Aerospace*, Vol. 9 No. 8, p. 438, doi: 10.3390/aerospace9080438.

Dessena, G., Civera, M., Ignatyev, D.I., Whidborne, J.F., Zanotti Fragonara, L. and Chiaia, B. (2023b), "The accuracy and computational efficiency of the Loewner framework for the system identification of mechanical systems", *Aerospace*, Vol. 10 No. 6, p. 571, doi: 10.3390/aerospace10060571.

Dessena, G., Pontillo, A., Ignatyev, D.I., Whidborne, J.F. and Zanotti Fragonara, L. (2024b), "A paradigm shift to assembly-like finite element model updating", *Journal of Vibration and Control*.

Dessena, G., Ignatyev, D.I., Whidborne, J.F. and Zanotti Fragonara, L. (2024c), "A kriging approach to model updating for damage detection", *Lecture Notes in Civil Engineering*, Springer International Publishing, 16 June, 2022, pp. 245-255, doi: 10.1007/978-3-031-07258-1_26.

Dessena, G., Ignatyev, D.I., Whidborne, J.F., Pontillo, A., Zanotti Fragonara, L. and Fragonara, L. (2022b), "Ground vibration testing of a high aspect ratio wing with revolving clamp", *33rd Congress of the International Council of the Aeronautical Sciences, ICAS 2022*, Vol. 6, pp. 4169-4181, doi: 10.17862/cranfield.rd.20486229.

Fan, W. and Qiao, P. (2011), "Vibration-based damage identification methods: a review and comparative study", *Structural Health Monitoring*, Vol. 10 No. 1, pp. 83-111, doi: 10.1177/1475921710365419.

Farrar, C.R., Doebling, S.W. and Nix, D.A. (2001), "Vibration–based structural damage identification", *Philosophical Transactions of the Royal Society of London. Series A: Mathematical, Physical and Engineering Sciences*, Vol. 359 No. 1778, pp. 131-149, doi: 10.1098/rsta.2000.0717.

Gosea, I.V. and Antoulas, A.C. (2015), "Model reduction of linear and nonlinear systems in the Loewner framework: a summary", *2015 European Control Conference (ECC)*, IEEE, pp. 345-349, doi: 10.1109/ECC.2015.7330568.

Grivet-Talocia, S. and Gustavsen, B. (2016), *Passive Macromodeling: Theory and Applications*, Wiley, doi: 10.1002/9781119140931.

Gustavsen, B. (2006), "Improving the pole relocating properties of vector fitting", 2006 IEEE Power Engineering Society General Meeting, Vol. 21, IEEE, p. 1, doi: 10.1109/PES.2006.1708940.

Gustavsen, B. and Semlyen, A. (1999), "Rational approximation of frequency domain responses by vector fitting", *IEEE Transactions on Power Delivery*, Vol. 14 No. 3, pp. 1052-1061, doi: 10.1109/61.772353.

Hayes, D., Pontillo, A., Yusuf, S.Y., Lone, M.M. and Whidborne, J. (2019), "High aspect ratio wing design using the minimum energy destruction principle", AIAA SciTech 2019 Forum, American Institute of Aeronautics and Astronautics, Kissimmee, FL, doi: 10.2514/6.2019-1592.

Kramer, B. and Gugercin, S. (2016), "Tangential interpolation-based eigensystem realization algorithm for MIMO systems", *Mathematical and Computer Modelling of Dynamical Systems, Taylor\& Francis*, Vol. 22 No. 4, pp. 282-306, doi: 10.1080/13873954.2016.1198389.

Lefteriu, S. and Antoulas, A.C. (2010), "A new approach to modeling multiport systems from frequency-domain data", *IEEE Transactions on Computer-Aided Design of Integrated Circuits and Systems*, Vol. 29 No. 1, pp. 14-27, doi: 10.1109/TCAD.2009.2034500.

Lefteriu, S. and Antoulas, A.C. (2009), "Modeling multi-port systems from frequency response data via tangential interpolation", 2009 IEEE Workshop on Signal Propagation on Interconnects, pp. 1-4, doi: 10.1109/SPI.2009.5089847.

Ljung, L. (1987), *System Identification: Theory for the User, First*, Prentice Hall, Englewood Cliffs, NJ.

Ljung, L., Chen, T. and Mu, B. (2020), "A shift in paradigm for system identification", *International Journal of Control, Taylor & Francis*, Vol. 93 No. 2, pp. 173-180, doi: 10.1080/00207179.2019.1578407.

Löwner, K. (1934), "Uber monotone matrixfunktionen", *Mathematische Zeitschrift*, Vol. 38 No. 1, pp. 177-216, doi: 10.1007/BF01170633.

Lubrina, P., Giclais, S., Stephan, C., Boeswald, M., Govers, Y. and Botargues, N. (2014), "AIRBUS A350 XWB GVT: state-of-the-art techniques to perform a faster and better GVT campaign", in Allemang, R. (Ed.), Topics in Modal Analysis II, Volume 8. *Conference Proceedings of the Society for Experimental Mechanics Series*, Vol. 45, *Springer*, Cham, Orlando, FL., pp. 243-256, doi: 10.1007/978-3-319-04774-4_24.

Maia, N.M.M. (1988), *Extraction of Valid Modal Properties from Measured Data in Structural Vibrations*, Imperial College London, London, available at: www.imperial.ac.uk/media/imperial-college/research-centres-and-groups/dynamics/40377708.PDF

Mayo, A.J.J. and Antoulas, A.C.C. (2007), "A framework for the solution of the generalized realization problem", *Linear Algebra and Its Applications*, Vol. 425 Nos 2/3, pp. 634-662, doi: 10.1016/j.laa.2007.03.008.

Mugnaini, V., Zanotti Fragonara, L. and Civera, M. (2022), "A machine learning approach for automatic operational modal analysis", *Mechanical Systems and Signal Processing*, Vol. 170, p. 108813, doi: 10.1016/j.ymssp.2022.108813.

Olejnik, A., Rogólski, R. and Szcześniak, M. (2022), "Application of the contact and non-contact measuring techniques for on-ground resonance testing of the mini-UAV", *Aircraft Engineering and Aerospace Technology*, Vol. 94 No. 1, pp. 89-98, doi: 10.1108/AEAT-12-2020-0327.

Pontillo, A. (2020), *High Aspect Ratio Wings on Commercial Aircraft: A Numerical and Experimental Approach*, Centre for Aeronautics, Cranfield University, Cranfield, UK, available at: https://dspace.lib.cranfield.ac.uk/handle/1826/20266

Pontillo, A., Hayes, D., Dussart, G.X., Lopez Matos, G.E., Carrizales, M.A., Yusuf, S.Y. and Lone, M.M. (2018), "Flexible high aspect ratio wing: low cost experimental model and computational framework", 2018 AIAA Atmospheric Flight Mechanics Conference, American Institute of Aeronautics and Astronautics, *Reston*, pp. 1-15, doi: 10.2514/6.2018-1014.

Prananta, B., Kanakis, T., Vankan, J. and van Houten, R. (2016), "Model updating of finite element model using optimisation routine", *Aircraft Engineering and Aerospace Technology*, Vol. 88 No. 5, pp. 665-675, doi: 10.1108/AEAT-02-2015-0064.

Promio, C.F., Samikkannu, R., Sura, N.K. and Mulla, S. (2018), "System identification-based aeroelastic modelling for wing flutter", *Aircraft Engineering and Aerospace Technology*, Vol. 90 No. 2, pp. 261-269, doi: 10.1108/AEAT-08-2016-0122.

Quero, D., Vuillemin, P. and Poussot-Vassal, C. (2019), "A generalized state-space aeroservoelastic model based on tangential interpolation", *Aerospace*, Vol. 6 No. 1, p. 9, doi: 10.3390/aerospace6010009.

Rytter, A.A. (1993), *Vibrational Based Inspection of Civil Engineering Structures*, Department of Building Technology and Structural Engineering, Aalborg University, Aalborg, Denmark, available at: https://vbn.aau.dk/en/publications/vibrational-based-inspection-of-civil-engineering-structures

Sibille, L., Civera, M., Zanotti Fragonara, L. and Ceravolo, R. (2023), "Automated operational modal analysis of a helicopter blade with a density-based cluster algorithm", *AIAA Journal*, Vol. 61 No. 3, pp. 1411-1427, doi: 10.2514/1.j062084.

Sohn, H., Farrar, C.R., Hemez, F., Czarnecki, J., Shunk, D.D., Stinemates, D.W., Nadler, B.R., *et al* (2004),. *A Review of Structural Health Monitoring Literature: 1996–2001*, Los Alamos, CA, available at: www.osti.gov/biblio/976152

Van Overschee, P. and De Moor, B. (1994), "N4SID: subspace algorithms for the identification of combined deterministic-stochastic systems", *Automatica*, Vol. 30 No. 1, pp. 75-93, doi: 10.1016/0005-1098(94)90230-5.

Weber, S., Kissinger, T., Chehura, E., Staines, S., Barrington, J., Mullaney, K., Fragonara, L.Z., Petrunin, I., James, S., Lone, M. and Tatam, R. (2021), "Application of fibre optic sensing systems to measure rotor blade structural dynamics", *Mechanical Systems and Signal Processing*, Vol. 158, p. 107758, doi: 10.1016/j.ymssp.2021.107758.

Yusuf, S.Y., Hayes, D., Pontillo, A., Carrizales, M.A., Dussart, G.X. and Lone, M.M. (2019), "Aeroelastic scaling for flexible high aspect ratio wings", AIAA SciTech 2019 Forum, American Institute of Aeronautics and Astronautics, *Reston*, pp. 1-14, doi: 10.2514/6.2019-1594.

Zanotti Fragonara, L., Boscato, G., Ceravolo, R., Russo, S., Ientile, S., Pecorelli, M.L. and Quattrone, A. (2017), "Dynamic investigation on the Mirandola bell tower in post-earthquake scenarios", *Bulletin of Earthquake Engineering*, Vol. 15 No. 1, pp. 313-337, doi: 10.1007/s10518-016-9970-z.

Appendix

The element mass and stiffness matrices for the 2D Euler Bernoulli beam considered are presented below. L is intended here as the length of a single element.

$$\mathbf{M}_e = \frac{\rho A L}{420}\begin{bmatrix} 156 & 22L & 54 & -13L \\ 22L & 4L^2 & 13L & -3L^2 \\ 54 & 13L & 156 & -22L \\ -13L & -3L^2 & -22L & 4L^2 \end{bmatrix} \tag{A1a}$$

$$\mathbf{K}_e = \begin{bmatrix} \frac{12EI}{L^3} & \frac{6EI}{L^2} & -\frac{12EI}{L^3} & \frac{6EI}{L^2} \\ \frac{6EI}{L^2} & \frac{4EI}{L} & -\frac{6EI}{L^2} & \frac{2EI}{L} \\ -\frac{12EI}{L^3} & -\frac{6EI}{L^2} & \frac{12EI}{L^3} & -\frac{6EI}{L^2} \\ \frac{6EI}{L^2} & \frac{2EI}{L} & -\frac{6EI}{L^2} & \frac{4EI}{L} \end{bmatrix} \tag{A1b}$$

Corresponding author

Marco Civera can be contacted at: marco.civera@polito.it and **Gabriele Dessena** can be contacted at: gdessena@ing.uc3m.es